Desalination and Water Treatment
www.deswater.com

doi: 10.5004/dwt.2018.22682

123 (2018) 196–202
August

Investigating the effects of Fe dopant on structural, optical, and photocatalytic properties of ZnO nanoflowers

L. Torkian[a,b], R. Azimirad[c], S. Safa[d,*]

[a]*Research Center of Modeling and Optimization in Science and Engineering, Islamic Azad University, South Tehran Branch, Tehran, Iran, email: ltorkian@gmail.com*
[b]*Department of Applied Chemistry, Islamic Azad University, South Tehran Branch, Tehran, Iran*
[c]*Nanophysics Group, Malek-Ashtar University of Technology, Tehran, Iran, email: azimirad@yahoo.com*
[d]*Young Researchers and Elite Club, South Tehran Branch, Islamic Azad University, Tehran, Iran, Fax: +982122974546; email: officialletters.safa@gmail.com*

Received 14 October 2017; Accepted 28 June 2018

ABSTRACT

Fe-doped ZnO nanostructures with various concentrations of Fe dopant (from 0 to 5 at.%) were synthesized by using a simple one-stage hydrothermal method. The structural characterization of the samples shows that Fe^{2+} is substituted in the cationic sites of ZnO wurtzite lattice structure. The optical band gap of the samples was a little decreased by increasing the concentration of Fe dopant (from 3.21 eV for bare ZnO to 2.92 eV for 5 at.% Fe-doped ZnO). This observation implies the formation of shallow levels within optical band gap and is confirmed by relative extinction of photoluminescence peaks with increasing the Fe content. On the other hand, the regular in shape nanoflowers seem to be the best choice for good light harvesting. Concerning the aforesaid affecting parameters, one can conclude that there must be an optimal concentration of Fe for having the maximum photocatalytic performance which was obtained to be 2 at.% Fe by photocatalytic tests.

Keywords: ZnO; Fe dopant; Nanoflower; Photocatalyst

1. Introduction

Studies on doped nanostructures have been preceded in photo-assisted applications because of having an important advantage known as tunable electronic band structure. Thus, various works on manipulating the optical band structure have been reported which are generally focused on either photogenerated electron/hole recombination inhibition or enhancing the density of carriers by incorporation of dopants [1–4]. Specifically, as a wide band gap semiconductor, ZnO has attracted a great deal of attentions to be utilized as an optical device in various fields such as photocatalyst material [5], ultraviolet (UV) detector [6], solar cell material [7], and light emitting diode [8].

Among them, photocatalysts, as eco-friendly materials, are important for environment-related applications because they can easily convert toxic chemicals (organic pollutants) into the water and nonharmful constituents by solar irradiation [9]. To more explain, the freed electron and holes (by photo-irradiation) react with water molecules and produce OH^- and O_2^- radicals [10]. These radical can convert toxic molecules to nontoxic ones.

Nevertheless, it is noteworthy that ZnO has no sensitivity against visible light and also, suffers from nearly fast recombination of photogenerated electron–hole pairs, which hinders its industrial application. Therefore, the density of recombination survived electron/hole pairs should be increased by adding shallow levels by various methods like adding structural defects [11] and/or dopants such as Co^{2+} [12], Mn^{2+} [13], Ni^{2+} [14], and Fe^{2+} [15,16].

* Corresponding author.

Concerning this aim, doping of Fe ions has been applied by many groups [15–18]. Huang et al. [17] indicated that Fe ions can effectively inhibit the electron–hole pair recombination by trapping the photogenerated electrons in added sublevels. Xiao et al. [18] observed the constructive effects of Fe dopant on the photocatalytic performance of ZnO nanorods in an optimum concentration of 1.0 at.%. In another work, Ba-Abbad et al. [19] extended the photocatalytic activity of ZnO to the visible range of light via Fe dopant. More recently, we observed that the presence of Fe dopant in the outer layer of ZnO nanorod (shell layer) can effectively improve both sensitivity and time of response of a ZnO-based UV detector [20,21]. These findings all imply that how Fe dopant can effectively inhibit electron/hole recombination [22].

On the other hand, Fe dopant in hydrothermal method may have some adverse effects especially on changing the porous microstructure to irregular one as it was observed by Hui et al. [23]. Hassanpour et al. [24] evaluated the incorporation of various cationic dopant and observed same results on variable morphology of ZnO nanostructure and attributed this observation to the variation of self-assembly parameters during hydrothermal equilibrium growth. Therefore, one can conclude that an optimum point between morphology and optical characteristics must be existed.

In fact, as it is clear, chemical synthesis method in the presence of cationic dopant can directly influence the characteristics of nanoparticles. Concerning this, it can be seen that various works are focused to find the best morphology of ZnO nanostructures [15–25] with optimized photo-related applications have been published. Thus, as we have seen interesting results of ZnO nanoflower in various fields [25,26], we tried to do a complementary work on optimizing this morphology by incorporation of Fe dopant. Concerning the advantages of nanoflower morphology, Jiang et al. [27] observed that nanoflowers, due to an amazing surface area, shows better proficiency for dyes loading and light harvesting even than nanorods in photo-assisted applications. Thus, one can see that Fe-doped ZnO nanoflowers may provide an optimized condition to be applied in practical photo-assisted applications and that's the objective of this study.

Owing to the importance of optical properties of photocatalytic materials, we tailored the photocatalytic properties to room temperatures photoluminescence (PL) in details.

2. Experimental details

2.1. Synthesis of Fe-doped flower-like ZnO

ZnO and Fe-doped ZnO nanostructures were prepared by a simple and easy-going hydrothermal process by using analytical-graded precursors. Firstly, 20 mL of a 1.0 M urea aqueous solution (as precipitation agent) was dripped into 25 mL of 0.1 M zinc nitrate aqueous solution under vigorous stirring until all reagents were dissolved completely. For the synthesis of Fe-doped ZnO samples, three batches with different amount of ferric nitrate (the atomic ratio of Fe to Zn was adjusted to be 0, 0.5, 2, and 5 at.%) were added into as previously prepared solutions, under constant stirring. The mixed solutions were all independently poured into a Teflon-lined stainless steel autoclave with 100 mL capacity and were held at the constant temperature of 120°C for 6 h. After the completion of the reactions, the resulting precipitates were centrifuged and then washed with absolute ethanol and distilled water for several times. Finally, the obtained white products were dried at 60°C and heat-treated at 400°C for 2 h in air. To evaluate the optical, structural, and photocatalytic properties of the obtained ZnO nanoflowers, the commercial ZnO nanopowder (20–30 nm, Teconan) was used as benchmark.

2.2. Physical characterization

The crystal structure of the samples was determined by X-ray diffractometry (XRD) by using an *Inel EQUINOX 3000* system in the range of 20°–75° with the step size of 0.1°. The morphologies of the ZnO nanopowders were depicted by scanning electron microscopy (VEGA TESCAN II). The optical transmittance of the ZnO powders in 320–900 nm range of wavelengths was carried out by using a diffuse reflectance spectroscopy (DRS, MPC-2200). Room temperature PL spectra were taken on a *Perkin-Elmer LS55* system equipped with a 450 W Xe lamp as an excitation source. A double-beam UV spectrophotometer (Shimadzu UV-1700) was used for indirect determination of *P*-nitrophenol (PNP) concentration in solution.

2.3. Photocatalytic analysis

In a typical process, the photocatalytic reaction was carried out by using a 50 mL of PNP (20 mg L^{-1}) solution, which was admixed with 0.05 g of photocatalyst powder in a 100 mL beaker as the photoreactor. Before irradiation, the photoreactor was stirred in the dark for 120 min to achieve an equilibrium point of physical adsorption of PNP molecules and also, measure the active surface area of powders through dye adsorption values in dark [28]. Then, the dark-remained photoreactor was irradiated with a combinatory of a 400 W tungsten light (as the source of visible light) and a 400 W high-pressure mercury lamp (as the UV light source). For determination of PNP degradation, 3 mL of each photoreacted solution was collected at specified periods, separated from the photocatalyst nanopowder by centrifugation and after that, its optical absorbance was taken. The photocatalytic performance of the samples was indirectly monitored by relating the amount of decolorizing to the degree of PNP degradation.

3. Results and discussion

The crystal structure of the synthesized samples is shown in Fig. 1. As can be seen, all of the samples are crystallized according to JCPDS no. 36-1451. Almost, no preferential orientation is observable for these samples. Also, the lack of any peaks except of ZnO phase shows that the concentration of impurities and/or unwanted Fe-based crystals is negligible (lesser than 4 at.%).

It is seen that the sharpness of peaks is a little decreased by adding Fe dopant into the ZnO lattice. Also, the lattice parameters were calculated and summarized in Table 1. As can be seen, the lattice parameters and also calculated volume of hexagonal unit-cell are slightly varied (a little increased

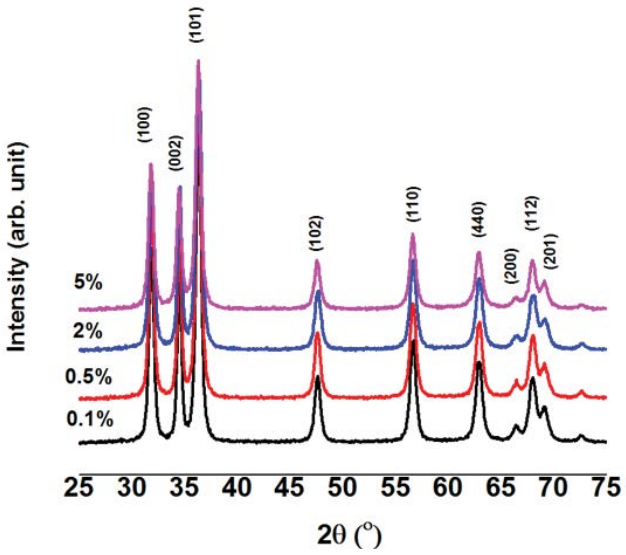

Fig. 1. XRD patterns of bare and Fe-doped ZnO nanostructures.

up to 5 at.% incorporation). This observation, indirectly, suggested us that probably Zn^{2+} (0.74 Å) is substituted by Fe^{2+} (0.76 Å) cationic sites [29].

The average grain size of the samples was calculated using standard Scherer's equation. The average grain size of the samples was considered as the average between three main peaks of (100), (002), and (101) and were obtained to be 32, 31, 30, and 30 for the samples containing 0.1, 0.5, 2.0, and 5.0 at.% Fe, respectively. The fair decrement of grain size can be explained by the very small difference between radii of Fe^{2+} and Zn^{2+} [23]. Accordingly, the lattice size of ZnO is almost unchanged by adding up the concentration of Fe atoms.

The morphology of as-synthesized pure and Fe-doped ZnO nanostructures is indicated in Figs. 2(a–e). Fig. 2(a) shows a flower-like morphology containing concentric scaled features. The SEM images shown in Fig. 2(a) suggest that nitrate anions in the presence of urea cause a spontaneous growth of crystallographic planes in more than one direction and so lead to the formation of regular-in-shape nanoflakes, which are bonded to each other to form a flower-like nanostructure [30]. The SEM pictures of the ZnO samples with 0.1, 0.5, 2, and 5 at.% Fe-doping are also shown in Figs. 2(b–e), respectively. There is a notable difference in morphology and size between the bare and 0.1 at.% Fe-doped ZnO with other samples as seen in Fig. 2. When the atomic percentage of Fe increases to 0.5 at.%, it can be clearly seen that the original nanoflowers are spoiled. Correspondingly, Han et al. [31] suggested that with increasing of the Fe content, the sheets are somewhat deteriorated, which is attributed to the incorporation of Fe ions [32].

The UV–Vis diffuse reflectance spectra (DRS) of the samples are exhibited in Fig. 3. As it is obvious the spectra reveal a characteristic absorption edge at the wavelength of ~380 nm corresponding to its band-to-band transition of ZnO. The optical band gap of the samples can be calculated from absorption plot by Tauc's relation $(\alpha h\upsilon)^n = A(h\upsilon - E_g)$ where α is the absorption coefficient, E_g is the optical band gap, A is a constant related to the effective mass, $h\upsilon$ is the photon energy, and n is the power depending upon the type of optical transition (n = 0.5 for indirect transition and 2 for direct one). Then, optical band gap (E_g) can be calculated through plotting the graph of $(\alpha h\upsilon)^2$ versus $h\upsilon$. The band gap energy of 0.1 at.% Fe-doped ZnO is found to be 3.21 eV and decreases very slightly with increasing the Fe content (summarized in Table 1).

The above results indicated that optical absorbance of the samples extends to visible light slightly by incorporation of Fe ions. The extended optical absorbance over the UV range can be exploited by the formation of new shallow levels due to sp-d exchange interactions in Fe-doped ZnO structure [33].

Figs. 4(a–e) show the PL spectra of the samples. ZnO by itself generates some constant emissions such as UV emission (~380 nm), green emission (~540 nm), and red emission (~630 nm) [34]. The 380 nm emission is generally assigned to free exciton recombination through an exciton–exciton collision process called near band edge emission [35] and underwent to a transition near 3.2 eV (optical band gap of ZnO). The low energy emissions at wavelengths between 500 and 650 nm are generally assigned to relaxation of electrons from various deep bands to valence band and generally come from the oxygen vacancies and incorporated dopants [36,37]. Therefore, the stronger the intensity of visible emission, the more defective the material is [38]. To have better judgments on data extracted from PL, the broad peak of each sample was deconvoluted by Lorentzian function to seven different subpeaks. As can be seen in Fig. 4, with an increment in Fe concentration, both of the exciton and defects originated peaks are attenuated and also, the UV emission peak is a little red-shifted. This means that Fe dopant narrows the optical band gap of ZnO which confirms the results of optical absorption spectra (see Fig. 3 and Table 1). Besides, the peaks intensity ratio of $I_{green}/I_{ultraviolet}$ is obtained to be 0.058 for bare

Table 1
The structural, optical, and photocatalytic properties of the bare and Fe-doped nanostructures

Sample	Band gap (eV)	Grain size (nm)	Photocatalytic constant (h^{-1})	Lattice parameters		
				$a = b$ (nm)	C (nm)	V (nm^3)
Bare ZnO	–	–	0.007	–	–	–
0.1 at.% Fe-doped ZnO	3.2 ± 0.096	33 ± 3.3	0.010	0.3241	0.5193	0.04723
0.5 at.% Fe-doped ZnO	3.1 ± 0.093	31 ± 3.1	0.019	0.3241	0.5193	0.04724
2 at.% Fe-doped ZnO	3.0 ± 0.09	30 ± 3.0	0.033	0.3241	0.5192	0.04723
5 at.% Fe-doped ZnO	2.9 ± 0.087	30 ± 3.0	0.019	0.3245	0.5199	0.0474

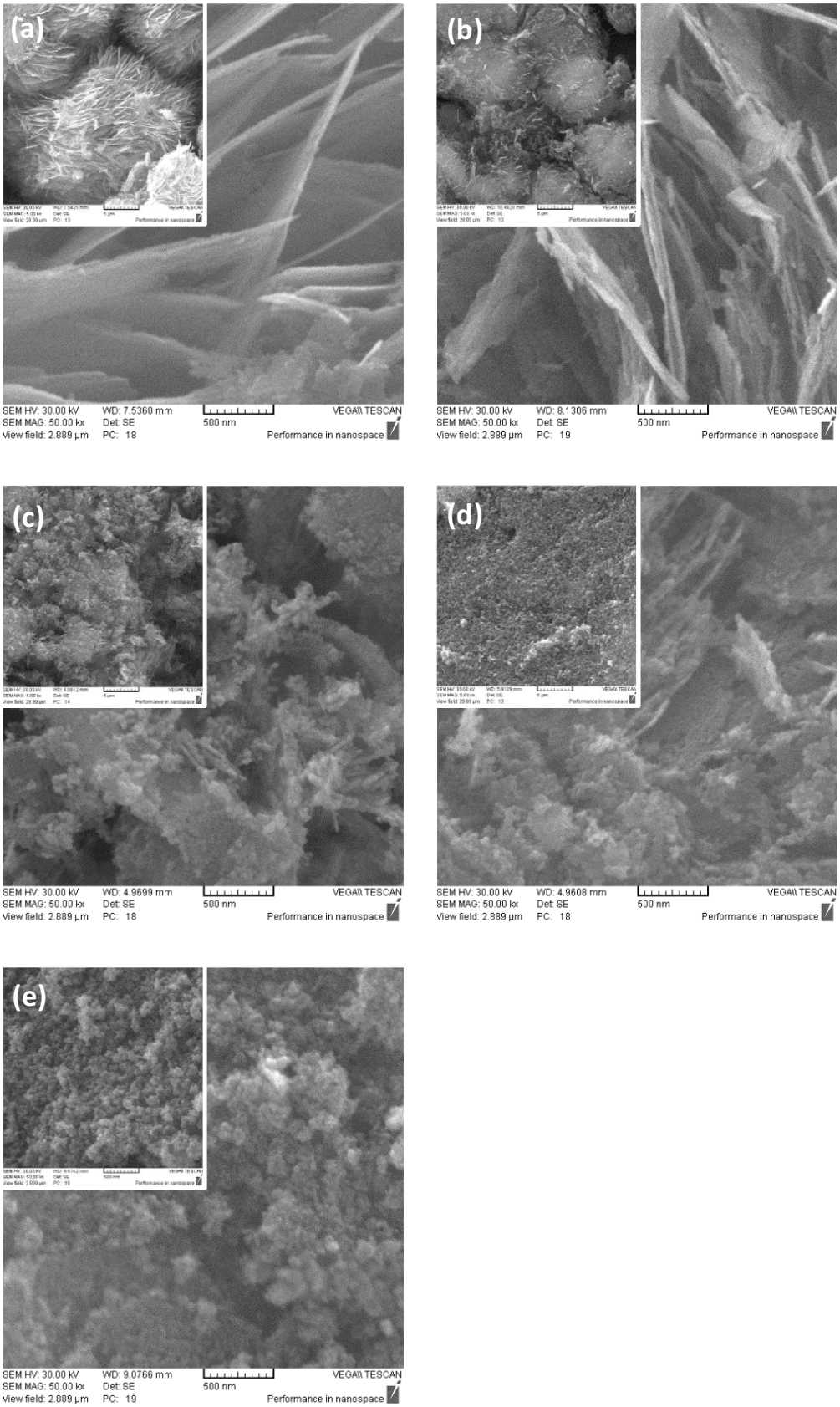

Fig. 2. SEM images of morphological evolution of ZnO nanostructures containing: (a) 0, (b) 0.1, (c) 0.5, (d) 2, and (e) 5 at.% Fe. The insets correspond to lower magnification images to have a better assessment on nanoparticles' distribution.

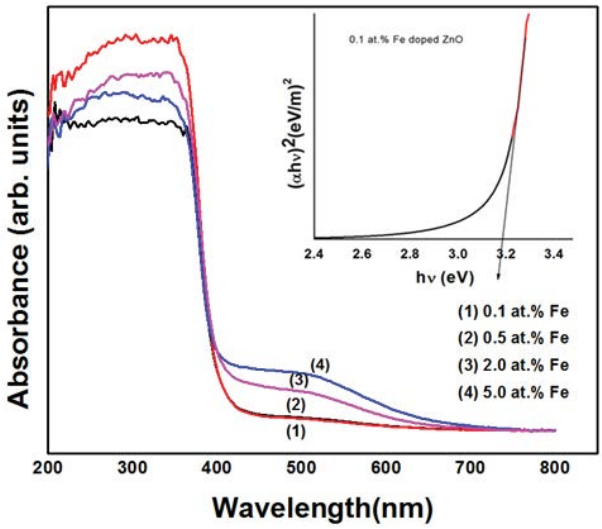

Fig. 3. The optical absorbance spectra of bare and Fe-doped ZnO nanostructures. The inset shows the calculated Tauc plot for determination of optical band gap of 0.1 at.% Fe-doped ZnO sample.

ZnO nanoflowers and is decreased slowly by increasing the content of Fe dopant. Therefore, one expects a low oxygen vacancy (as well as Zn interstitial) concentration by increment of Fe dopant in ZnO lattice structure.

The rate of PNP degradation was calculated through PNP decolorization and is shown in Fig. 5. As can be seen, the power of photocatalysts has logarithmic behavior and the plot of $\ln(C_0/C)$ against irradiation time is well fitted by a linear equation. The slope of this plot is generally considered as the photocatalytic constant. As can be seen, in our arranged condition, the sample containing 2 at.% of Fe dopant shows the strongest photocatalytic performance among the samples.

Generally, the photocatalytic property is a function of (1) physical properties of the sample like surface area and (2) intrinsic properties of material like optical band gap and effective life of electron/hole pairs. Herein, PL spectra show that incorporation of Fe dopant can effectively inhibit the electron/hole recombination (by the relative extinction of PL peak) and thus, is favorable to be incorporated in ZnO-based photocatalyst. This claim is in good relation with the increment of photocatalytic rate constant (within Fig. 5). On the other hand, the regular in-shape porous structure of ZnO is

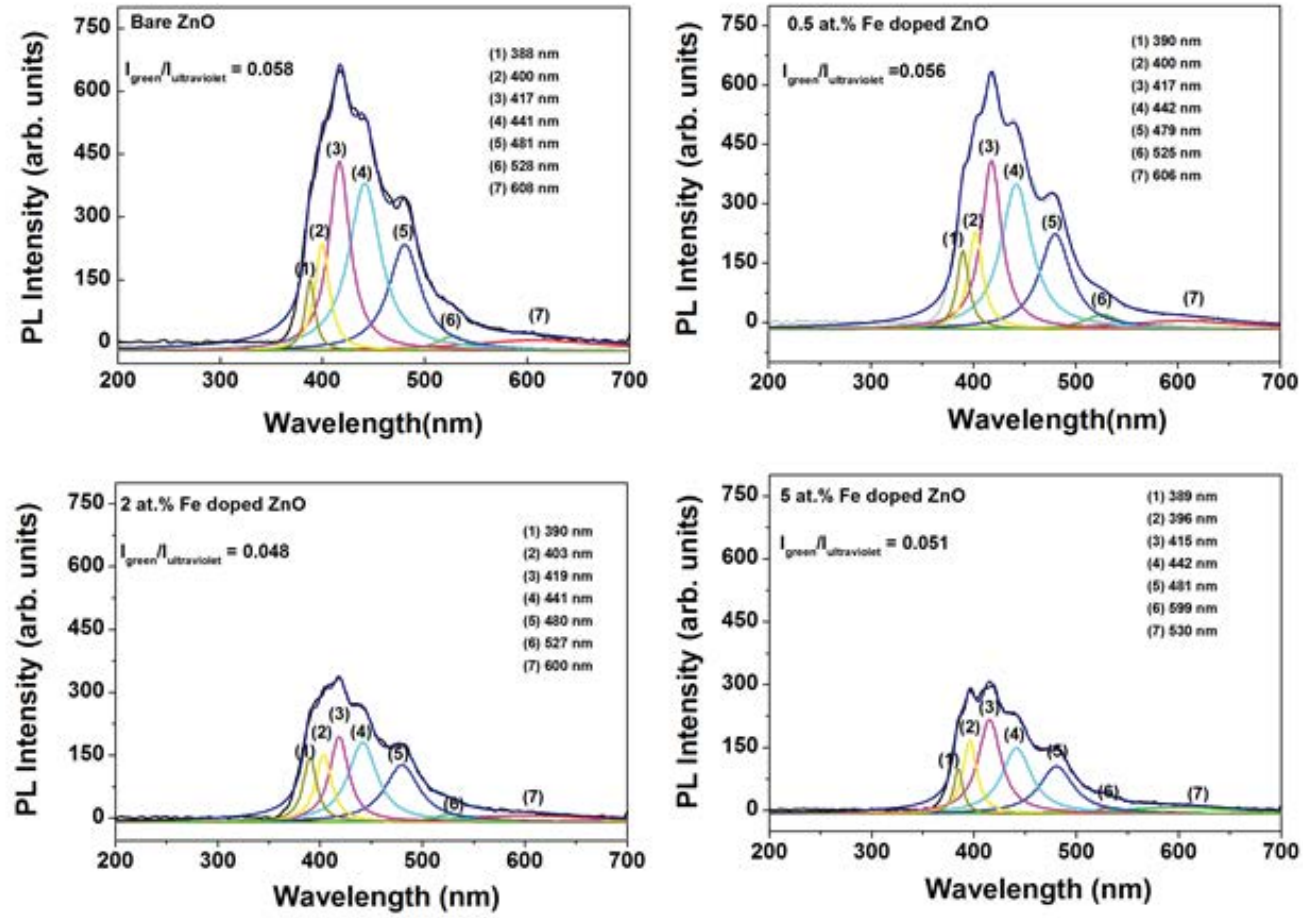

Fig. 4. Photoluminescence spectra of bare and Fe-doped ZnO nanostructures. The PL peaks are deconvoluted according to Lorentzian function.

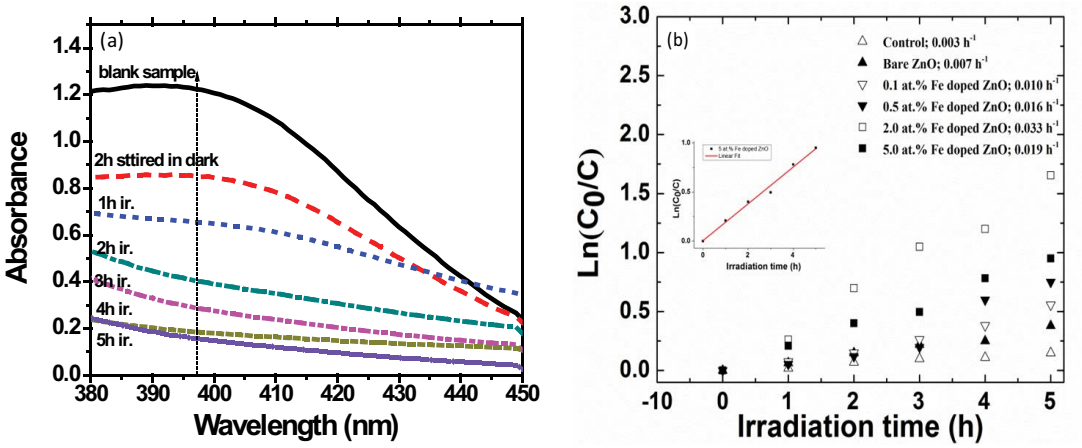

Fig. 5. (a) The UV-visible optical spectra relating to variation of *P*-nitrophenol concentration for 2 at.% Fe-doped ZnO sample and (b) the pseudo-first-order linear fitting of the photocatalytic results and derived apparent kinetic rate constants. The inset shows a typical linear fitting for computing of kinetic rate constants.

slowly out-fashioning by increment of Fe (especially at values ≥0.5 at.% according to SEM images in Fig. 2) until the formation of a completely irregular morphology (which suffers from agglomeration) for 5 at.% Fe sample. Therefore, one should expect an optimum point for Fe percentage in ZnO lattice and here, is found to be 2 at.%.

4. Conclusions

The Fe-doped ZnO nanostructures were synthesized by a simple hydrothermal method. The lack of any XRD peaks shifting revealed that Fe^{2+} ionic state (with nearly close ionic radius with Zn^{2+}) is probably substituted instead of Zn^{2+} in ZnO lattice structure. Nevertheless, Fe^{2+} dopant has substantial effects on morphological and optical properties of ZnO. In fact, by an increment of Fe dopant, the morphology of bare ZnO is completely degraded from regular nanoflowers to agglomerated nanoparticles. Moreover, the addition of shallow levels due to the increment of Fe^{2+} within optical band gap caused a kind of decrement of band gap from 3.21 to 2.92 eV. Considering these data, it is logical that an optimum point for dopant content should exist. By comparing the data of photocatalytic degradation of PNP, it was shown that 2 at.% Fe-doped ZnO sample is the optimal point for photocatalytic performance and its photocatalytic constant rate is about five times greater than that of bare ZnO nanoflower sample.

References

[1] K. Vanheusden, W.L. Warren, J.A. Voigt, C.H. Seager, D.R. Tallant, Impact of Pb doping on the optical and electronic properties of ZnO powders, Appl. Phys. Lett., 67 (1995) 1280–1282.
[2] R. Wang, J.H. Xin, Y. Yang, H. Liu, L. Xu, J. Hu, The characteristics and photocatalytic activities of silver doped ZnO nanocrystallites, Appl. Surf. Sci., 227 (2004) 312–317.
[3] S. Sapra, D.D. Sarma, Evolution of the electronic structure with size in II-VI semiconductor nanocrystals, Phys. Rev. B, 69 (2004) 125304.
[4] G. Pozina, L.-L. Yang, Q.X. Zhao, L. Hultman, P.G. Lagoudakis, Size dependent carrier recombination in ZnO nanocrystals, Appl. Phys. Lett., 97 (2010) 131909.
[5] B. Li, Y. Wang, Facile synthesis and enhanced photocatalytic performance of flower-like ZnO hierarchical microstructures, J. Phys. Chem. C, 114 (2009) 890–896.
[6] H. Kind, H. Yan, B. Messer, M. Law, P. Yang, Nanowire ultraviolet photodetectors and optical switches, Adv. Mater., 14 (2002) 158.
[7] D. Wu, Z. Gao, F. Xu, J. Chang, W. Tao, J. He, S. Gao, K. Jiang, Hierarchical ZnO aggregates assembled by orderly aligned nanorods for dye-sensitized solar cells, CrystEngComm, 15 (2013) 1210–1217.
[8] C. Zhang, J. Lin, Defect-related luminescent materials: synthesis, emission properties and applications, Chem. Soc. Rev., 41 (2012) 7938–7961.
[9] M.R. Hoffmann, S.T. Martin, W. Choi, D.W. Bahnemann, Environmental applications of semiconductor photocatalysis, Chem. Rev., 95 (1995) 69–96.
[10] M. Cho, H. Chung, W. Choi, J. Yoon, Linear correlation between inactivation of *E. coli* and OH radical concentration in TiO_2 photocatalytic disinfection, Water Res., 38 (2004) 1069–1077.
[11] A. Khayatian, M. Almasi Kashi, R. Azimirad, S. Safa, S.F. Akhtarianfar Akhtarian, Effect of annealing process in tuning of defects in ZnO nanorods and their application in UV photodetectors, Optik, 127 (2016) 4675–4681.
[12] X.C. Liu, E.-W. Shi, Z.-Z. Chen, H.-W. Zhang, L.-X. Song, H. Wang, S.-D. Yao, Structural, optical and magnetic properties of Co-doped ZnO films, J. Cryst. Growth, 296 (2006) 135–140.
[13] R. Ullah, J. Dutta, Photocatalytic degradation of organic dyes with manganese-doped ZnO nanoparticles, J. Hazard. Mater., 156 (2008) 194–200.
[14] E. Liu, P. Xiao, J.S. Chen, B.C. Lim, L. Li, Ni doped ZnO thin films for diluted magnetic semiconductor materials, Curr. Appl. Phys., 8 (2008) 408–411.
[15] H. Liu, J. Yang, Y. Zhang, L. Yang, M. Wei, X. Ding, Structure and magnetic properties of Fe-doped ZnO prepared by the sol–gel method, J. Phys.: Condens. Matter, 21 (2009) 145803.
[16] J.T. Luo, Y.C. Yang, X.Y. Zhu, G. Chen, F. Zeng, F. Pan, Enhanced electromechanical response of Fe-doped ZnO films by modulating the chemical state and ionic size of the Fe dopant, Phys. Rev. B, 82 (2010) 014116.
[17] W. Huang, X. Tang, I. Felner, Y. Koltypin, A. Gedanken, Preparation and characterization of Fe_xO_y–TiO_2 via sono-chemical synthesis, Mater. Res. Bull., 37 (2002) 1721–1735.
[18] S. Xiao, L. Zhao, J. Lian, Enhanced photocatalytic performance of supported Fe doped ZnO nanorod arrays prepared by wet chemical method, Catal. Lett., 144 (2014) 347–354.

[19] M.M. Ba-Abbad, A.A.H. Kadhum, A.B. Mohamad, M.S. Takriff, K. Sopian, Visible light photocatalytic activity of Fe^{3+}-doped ZnO nanoparticle prepared via sol–gel technique, Chemosphere, 91 (2013) 1604–1611.
[20] R. Azimirad, A. Khayatian, M. Almasi Kashi, S. Safa, Electrical investigation and ultraviolet detection of ZnO nanorods encapsulated with ZnO and Fe-doped ZnO layer, J. Sol-Gel Sci. Technol., 71 (2014) 540–548.
[21] R. Azimirad, A. Khayatian, S. Safa, M. Almasi Kashi, Enhancing photoresponsivity of ultra violet photodetectors based on Fe doped ZnO/ZnO shell/core nanorods, J. Alloys Compd., 615 (2014) 227–233.
[22] Z.C. Chen, L.J. Zhuge, X.M. Wu, Y.D. Meng, Initial study on the structure and optical properties of $Zn_{1-x}Fe_xO$ films, Thin Solid Films, 515 (2007) 5462–5465.
[23] A. Hui, J. Ma, J. Liu, Y. Bao, J. Zhang, Morphological evolution of Fe doped sea urchin-shaped ZnO nanoparticles with enhanced photocatalytic activity, J. Alloys Compd., 696 (2017) 639–647.
[24] A. Hassanpour, P. Guo, S. Shen, P. Bianucci, The effect of cation doping on the morphology, optical and structural properties of highly oriented wurtzite ZnO-nanorod arrays grown by a hydrothermal method, Nanotechnology, 28 (2017) 435707.
[25] S. Safa, R. Azimirad, K. Mohammadi, R. Hejazi, A. Khayatian, Investigation of ethanol vapor sensing properties of ZnO flower-like nanostructures, Measurement, 73 (2015) 588–595.
[26] S. Safa, M. Khajeh, R. Azimirad, The effects of measuring atmosphere on ultraviolet photodetection performance of ZnO nanostructures, J. Alloys Compd., 735 (2018) 1406–1413.
[27] C.Y. Jiang, X.W. Sun, G.Q. Lo, D.L. Kwong, J.X. Wang, Improved dye-sensitized solar cells with a ZnO-nanoflower photoanode, Appl. Phys. Lett., 90 (2007) 263501.
[28] J.J. Kipling, R.B. Wilson, Adsorption of methylene blue in the determination of surface areas, J. Chem. Technol. Biotechnol., 10 (1960) 109–113.
[29] I. Soumahoro, R. Moubah, G. Schmerber, S. Colis, M. Ait Aouaj, M. Abd-Lefdil, N. Hassanain, A. Berrada, A. Dinia, Structural, optical, and magnetic properties of Fe-doped ZnO films prepared by spray pyrolysis method, Thin Solid Films, 518 (2010) 4593–4596.
[30] Q. Zhu, J. Chen, Q. Zhu, Y. Cui, L. Liu, B. Li, X. Zhou, Monodispersed hollow microsphere of ZnO mesoporous nanopieces: preparation, growth mechanism and photocatalytic performance, Mater. Res. Bull., 45 (2010) 2024–2030.
[31] L. Han, D. Wang, Y. Lu, T. Jiang, B. Liu, Y. Lin, Visible-light-assisted HCHO gas sensing based on Fe-doped flowerlike ZnO at room temperature, J. Phys. Chem. C, 115 (2011) 22939–22944.
[32] A. Yu, J. Qian, H. Pan, Y. Cui, M. Xu, L. Tu, Q. Chai, X. Zhou, Micro-lotus constructed by Fe-doped ZnO hierarchically porous nanosheets: preparation, characterization and gas sensing property, Sens. Actuators, B, 158 (2011) 9–16.
[33] S. Kumar, S. Basu, B. Rana, A. Barman, S. Chatterjee, S.N. Jha, D. Bhattacharyya, N.K. Sahoo, A.K. Ghosh, Structural, optical and magnetic properties of sol–gel derived ZnO:Co diluted magnetic semiconductor nanocrystals: an EXAFS study, J. Mater. Chem. C, 2 (2014) 481–495.
[34] A. Ghosh, N.G. Deshpande, Y.G. Gudage, R.A. Joshi, A.A. Sagade, D.M. Phase, R. Sharma, Effect of annealing on structural and optical properties of zinc oxide thin film deposited by successive ionic layer adsorption and reaction technique, J. Alloys Compd., 469 (2009) 56–60.
[35] W. Shan, W. Walukiewicz, J.W. Ager, K.M. Yu, H. Yuan, H.P. Xin, G. Cantwell, J.J. Song, Nature of room-temperature photoluminescence in ZnO, Appl. Phys. Lett., 86 (2005) 191911–191913.
[36] J. Zhang, L.D. Sun, C.S. Liao, C.H. Yan, A simple route towards tubular ZnO, Chem. Commun., 3 (2002) 262–263.
[37] C.-L. Hsu, Y.D. Gao, Y.-S. Chen, T.J. Hsueh, Vertical p-type Cu-doped ZnO/n-type ZnO homojunction nanowire-based ultraviolet photodetector by the furnace system with hotwire assistance, ACS Appl. Mater. Interfaces, 6 (2014) 4277–4285.
[38] S.K. Panda, C. Jacob, Preparation of transparent ZnO thin films and their application in UV sensor devices, Solid-State Electron., 73 (2012) 44–50.